High-resolution laser excitation spectroscopy of the $\tilde{A}\,^2E$-$\tilde{X}\,^2A_1$ transition of $SrCH_3$

M. J. Dick
Department of Physics, University of Waterloo, Waterloo, Ontario N2L 3G1, Canada

P. M. Sheridan and J.-G. Wang
Department of Chemistry, University of Waterloo, Waterloo, Ontario N2L 3G1, Canada

P. F. Bernath[a)]
Department of Physics, University of Waterloo, Waterloo, Ontario N2L 3G1, Canada, and Department of Chemistry, University of Waterloo, Waterloo, Ontario N2L 3G1, Canada

(Received 7 February 2006; accepted 28 February 2006; published online 4 May 2006)

High-resolution laser excitation spectroscopy has been used to record the $\tilde{A}\,^2E$-$\tilde{X}\,^2A_1$ electronic transition of $SrCH_3$ in a laser ablation/molecular jet source. Transitions arising from the $K'=1 \leftarrow K''=0$, $K'=0 \leftarrow K''=1$, and $K'=2 \leftarrow K''=1$ subbands have been observed and assigned. The data were modeled with ^2E and $^2A_1$ symmetric top Hamiltonian matrices in a Hund's case (a) basis, using a least squares fitting program. Rotational and fine structure parameters for the $\tilde{A}\,^2E$ state were determined. A comparison of the spin-orbit energy separation in the $\tilde{A}\,^2E$ state to other strontium containing free radicals showed that the Jahn-Teller effect is negligible. The spin-rotation constants for the $\tilde{A}\,^2E$ state were calculated using the pure precession model and were found to be in good agreement with the experimentally determined parameters. These calculations suggest that the $\tilde{A}\,^2E$ state of $SrCH_3$ is not entirely of p orbital character. The rotational constants were used to estimate the structural parameters of $SrCH_3$ in the $\tilde{A}\,^2E$ state. The strontium-carbon bond length was found to decrease by $\sim$0.006 Å, and the hydrogen-carbon-hydrogen bond angle opened by $\sim$0.8° compared to the $\tilde{X}\,^2A_1$ state, similar to the geometry changes observed for $CaCH_3$.
 [DOI: 10.1063/1.2189236]

I. INTRODUCTION

Small alkaline-earth-containing molecules have been a favorite subject of gas phase spectroscopists over the past 30 years.[1,2] These species have been of particular interest because their bonding can be described simply as ionic [M^+ (metal atom) L^- (ligand)], with electronic states derived from the promotion of an unpaired electron residing in orbitals located primarily on the metal atom. The majority of the high-resolution studies of alkaline-earth-containing molecules have focused on diatomic metal halides and linear hydroxides. Polyatomic analogs with lower symmetry, however, have generally only been investigated at low or medium resolution due to the increasingly complicated appearance of their molecular spectra. These complexities are a result of additional interactions not present in the linear species. For example, nonlinear molecules in orbitally degenerate states may be subject to not only spin-orbit coupling, but also the Jahn-Teller effect, in which the molecule distorts to a nonsymmetric geometry to remove the orbital degeneracy.[3] This distortion will in turn alter the energies of the vibrational and rotational levels of the molecule.

Symmetric top molecules in orbitally degenerate states (E symmetry) may be subject to distortions due to the Jahn-Teller interaction. The effects on the rotational levels of such molecules were first explored by Brown[4] and later by Hougen[5] and Watson.[6] Brown derived the first effective Hamiltonian for a molecule in ^2E state, while Hougen expanded this expression to include additional terms caused by the Jahn-Teller effect. In addition, Hougen showed that the Jahn-Teller interaction can contribute to the values of the various rotational parameters of ^2E state. The first high-resolution experimental observation of a molecule in ^2E state was performed by King and Warren in 1969 on FSO_3.[7] This investigation was followed by the landmark study of the $\tilde{X}\,^2E$ state of CH_3O by Endo *et al.*[8] using microwave spectroscopy. In their analysis, they successfully applied the effective Hamiltonians of Brown and Hougen to the ground state of the methoxy radical. This work has been followed by high-resolution studies of CH_3O,[9–12] CH_3S,[13] and C_5H_5,[14] all of which have ^2E electronic ground states.

Another group of molecules in which ^2E electronic states are present are the metal monomethyls and monomethoxides. To date, the $\tilde{A}\,^2E$ states of $MgCH_3$,[15] $CaCH_3$,[16,17] $CaOCH_3$,[18,19] $SrOCH_3$,[20] $ZnCH_3$,[21] and $CdCH_3$[21,22] have been investigated at high resolution. For these molecules, spin-orbit coupling has been found to dominate over the Jahn-Teller interaction in the lowest vibrational level of the $\tilde{A}\,^2E$ state. In addition, the contribution of the

[a)]Author to whom correspondence should be addressed. Fax: 519-746-0435. Electronic mail: bernath@uwaterloo.ca

Jahn-Teller effect to the rotational parameters of the $\tilde{A}\,^2E$ states of these molecules has been shown to be far outweighed by interactions with other nearby excited states. Spectroscopic results concerning molecules with ^2E states have been reviewed by Barckholtz and Miller.[23]

In order to further investigate molecules in ^2E states and to continue our studies of alkaline earth monomethyls, we have recorded high-resolution spectra of the $\tilde{A}\,^2E$-$\tilde{X}\,^2A_1$ transition of $SrCH_3$. This investigation completes the high-resolution rotational analysis of the low-lying $\tilde{A}\,^2E$ and $\tilde{B}\,^2A_1$ states of $CaCH_3$ and $SrCH_3$.[16,17,24] The fine structure parameters and the Jahn-Teller interaction in the $\tilde{A}\,^2E$ state of $SrCH_3$, in addition to the geometric parameters in these low-lying states, will be discussed.

II. EXPERIMENT

$SrCH_3$ was produced in the gas phase using a laser ablation/molecular jet source.[25] In this apparatus, a gas mixture of 1% tetramethyl tin in Ar, at a backing pressure of 100 psi, is introduced into a reaction nozzle assembly via a pulsed valve. As the gas mixture passes in front of a strontium target rod, the third harmonic (355 nm) of a pulsed (10 Hz) Nd/YAG (YAG denotes yttrium aluminum garnet) laser (10 mJ/pulse) strikes the metal surface to produce strontium vapor. In the resulting high energy plasma, $SrCH_3$ forms and exits the nozzle assembly into a low pressure chamber ($\sim 1\times 10^{-7}$ torr) to form a molecular jet ($T_{\mathrm{Rot}}\sim 4-6$ K). The molecules are probed perpendicular to the jet ~15 cm downstream with a visible laser. A photomultiplier tube (PMT), located perpendicular to the jet, is used to collect any resulting fluorescence. Band pass filters (±20 nm), centered on the probe laser frequency, are used to attenuate radiation from the plasma emission. The collected fluorescence signal is sent from the PMT, through a preamplifier (100× current), to a boxcar integrator. The laser excitation spectrum is then plotted as total fluorescence signal versus probe laser wavenumber.

In this study two high-resolution ring laser systems were used to obtain the rotationally resolved spectra of the two spin-orbit components of the $\tilde{A}\,^2E$-$\tilde{X}\,^2A_1$ transition of $SrCH_3$, based on the previous low-resolution work.[26] For the $\tilde{A}\,^2E_{1/2}$-$\tilde{X}\,^2A_1$ spin-orbit component (~13 655 cm^{-1}), a Coherent 899-29 titanium sapphire ring laser system (line width ~10 MHz) was utilized. Spectra were recorded in 5 cm^{-1} segments at a scan speed of 60 s/cm^{-1} with a data sampling interval of 10 MHz. The I_2 spectrum was recorded simultaneously in absorption to calibrate the line positions.[27] For the $\tilde{A}\,^2E_{3/2}$-$\tilde{X}\,^2A_1$ spin-orbit component (~13 935 cm^{-1}), a Coherent 699-29 ring dye laser system (line width ~10 MHz) operating with DCM laser dye was employed. Spectra were acquired by averaging together several (2–4) 5 cm^{-1} segments obtained at a scan speed of 180 s/cm^{-1}, with a data sampling interval of 10 MHz. The laser excitation spectrum of I_2 was measured simultaneously to calibrate the line positions.[28] The slower scan speed and segment averaging used to record spectra of this spin-orbit component were necessary to achieve an adequate signal-to-noise ratio. The decrease in signal strength observed for the $\tilde{A}\,^2E_{3/2}$-$\tilde{X}\,^2A_1$ transition can be attributed to several factors including lower output power of the dye laser in this spectral region and the degradation of the Sr rod during the experiment. For both spin-orbit components experimental line widths of ~350 MHz were observed due to residual Doppler broadening of the molecular jet as it interacts with the probe laser.

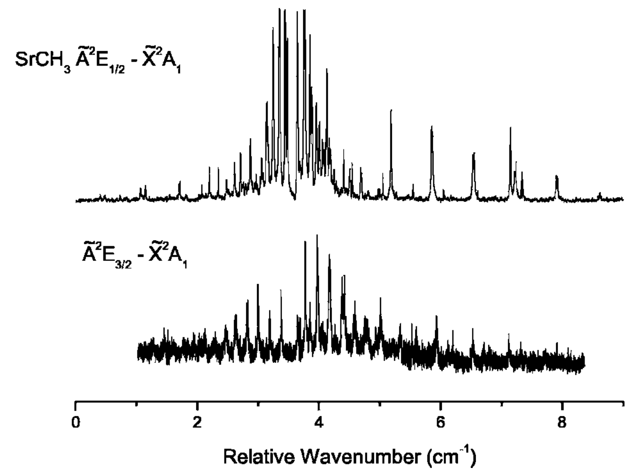

FIG. 1. Overall high-resolution spectra of the $\tilde{A}\,^2E$-$\tilde{X}\,^2A_1$ transition of $SrCH_3$. The $\tilde{A}\,^2E_{1/2}$-$\tilde{X}\,^2A_1$ (top panel) and $\tilde{A}\,^2E_{3/2}$-$\tilde{X}\,^2A_1$ (bottom panel) spin-orbit components are plotted on a relative wavenumber axis for comparison. Both spectra have the general appearance of a perpendicular type transition with ~1B and ~3B spaced branches. Transitions originating from both $K''=0$ and 1 levels of the $\tilde{X}\,^2A_1$ state are present with similar band origins, resulting in the congested appearance of the spectra.

III. RESULTS

$SrCH_3$ is a prolate symmetric top molecule belonging to the C_{3v} point group. The $\tilde{A}\,^2E$-$\tilde{X}\,^2A_1$ transition of this molecule corresponds to a $p\pi \leftarrow s\sigma$ type promotion of the unpaired electron located on the strontium atom. Figure 1 shows the overall spectrum obtained for the two spin-orbit components of the $\tilde{A}\,^2E$-$\tilde{X}\,^2A_1$ transition of $SrCH_3$. The appearance of this transition is similar to a $^2\Pi$-$^2\Sigma^+$ perpendicular type transition of a linear molecule such as SrCCH (Ref. 29) with ~1B and ~3B spaced branches present. The lower molecular symmetry of $SrCH_3$, however, results in a more complicated spectral pattern.

The energy levels of the $\tilde{A}\,^2E$ state can be labeled according to a Hund's case (a) coupling scheme.[4,16,17] In this case, the rotational angular momentum of the nuclei is represented by **R** and its projection on the symmetry axis (Sr–C bond) is indicated by K_R (all angular momenta components are given in units of $\hbar$). The projection of the orbital angular momentum **L** onto the symmetry axis is given by ζ_e. The off-axis protons of the methyl group are not expected to quench the orbital angular momentum of the unpaired electron significantly; therefore, ζ_e should be close to 1, because the ^2E state correlates with a $^2\Pi$ term in the linear limit. The projections K_R and ζ_e add along the symmetry axis to form K ($K=K_R+\zeta_e$). It should be noted that K_R, ζ_e, and K are all signed quantities and as a result each K level occurs as a degenerate pair. For example, if $K_R=0$ and $\zeta_e=\pm 1$, then two levels labeled as $K=\pm 1$ result. In the $\tilde{X}\,^2A_1$ state the value of ζ_e is zero, thus $K=K_R$ ($K=0$ is not degenerate in this state). In this paper, rotational levels will be labeled by $|K|$. The selection rule on K is $\Delta K=\pm 1$ ($\Delta K_R=0$) (Ref. 17) and as a result rotational lines can be grouped into ΔK subbands, for example $K'=0\leftarrow K''=1$ ($K'_R=1\leftarrow K''_R=1$). (Energy diagrams of the K level structure can be found in Refs. 16 and 17.) One final interaction that needs be considered concerns the coupling of K and Σ (the projection of the electron spin angular momentum $\mathbf{S}$ onto the symmetry axis) to give P ($P=K\pm\Sigma$) the projection of $\mathbf{J}$ ($\mathbf{J}=\mathbf{R}+\mathbf{L}+\mathbf{S}$), the total angular momentum, onto the symmetry axis. P, like Ω in a linear molecule, defines the minimum value of J ($J\geqslant P$) in a particular K group of rotational lines, which in turn determines the first rotational lines of a given ΔK subband.

Rotation of $SrCH_3$ about the symmetry axis results in the exchange of the three protons of the methyl group. As a consequence two nuclear spin states arise: *ortho* ($K=3N$, where N is an integer) and *para* ($K\neq 3N$).[30] The existence of two nuclear spin states affects the rotational cooling of the molecules in the free jet expansion because *ortho* and *para* molecules behave like separate species and cannot cool into one another. As a result of this phenomenon both the $K''=0$ and $K''=1$ levels are populated in the jet. Therefore, transitions arising from three subbands are expected to be the most intense in our spectra: $K'=1\leftarrow K''=0$, $K'=0\leftarrow K''=1$, and $K'=2\leftarrow K''=1$.

Energy level diagrams for the three ΔK subbands present in the $\tilde{A}\,^2E$-$\tilde{X}\,^2A_1$ spectrum of $SrCH_3$ have been included to more clearly illustrate the transitions observed and we have used them to guide our analysis. The $K'=1\leftarrow K''=0$, $K'=0\leftarrow K''=1$, and $K'=2\leftarrow K''=1$ subbands are shown in Figs. 2–4, respectively. In each diagram, the rotational levels in both the excited and ground electronic states are labeled by J. The unpaired electron, located on the strontium atom, causes each of the electronic states to be split into two spin components. In the $\tilde{X}\,^2A_1$ state, this splitting is due to the electron spin-rotation interaction, and in a parity basis the rotational levels of e parity are labeled as F_1 and those with f parity are identified as F_2. In the $\tilde{A}\,^2E$ state, the splitting is predominately due to the spin-orbit interaction and gives rise to the $^2E_{1/2}(F_1)$ and $^2E_{3/2}(F_2)$ spin-orbit components. The rotational levels in the upper state can be further split into e and f parity components similar to Λ-type doubling in linear molecules.[5] This splitting is resolvable for the $K'=1$ rotational levels, however, for the $K'=0$ or $K'=2$ ($K_R=1$) levels it is predicted to be negligible.[4,5] In each ΔK subband the allowed transitions are governed by the selection rule $\Delta J=0,\pm 1$. Each branch is labeled by the notation $^{\Delta K}\Delta J_{F'_iF''_j}$ ($i=1,2$; $j=1,2$), where ΔK is indicated using a lower case r or p.[4] In these three ΔK subbands a total of 36 branches are possible and expected in our spectra.

Line assignments of the $\tilde{A}\,^2E$-$\tilde{X}\,^2A_1$ transition were made by initially identifying series of branches in the $\tilde{A}\,^2E_{1/2}$-$\tilde{X}\,^2A_1$ spin-orbit component. Branch identifications were aided by using the $\tilde{A}\,^2E_{1/2}$-$\tilde{X}\,^2A_1$ transition of $CaCH_3$ as a guide.[17] Lower state combination differences[31] were then

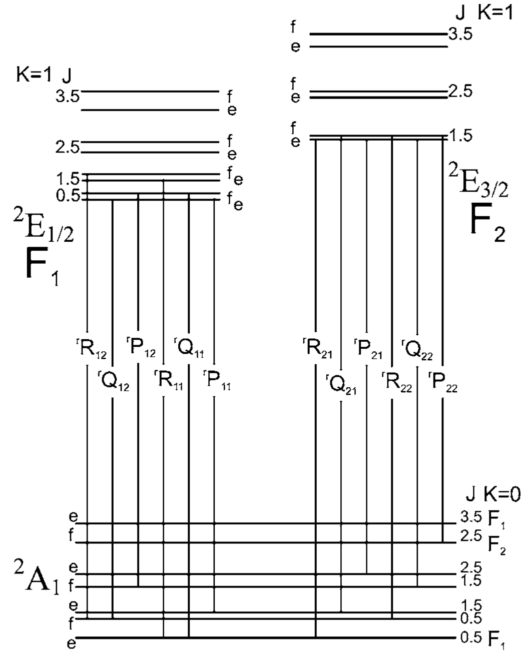

FIG. 2. An energy level diagram of the $K'=1\leftarrow K''=0$ subband of the $\tilde{A}\,^2E$-$\tilde{X}\,^2A_1$ transition of $SrCH_3$. The rotational energy levels are labeled by the symmetric top quantum numbers J and K. In the $\tilde{X}\,^2A_1$ state each rotational level is split by the spin-rotation interaction into two spin components labeled F_1 (e parity) and F_2 (f parity). In the $\tilde{A}\,^2E$ state, spin-orbit coupling results in $^2E_{1/2}$ (F_1) and $^2E_{3/2}$ (F_2) sublevels. In addition, each rotational level of the $\tilde{A}\,^2E$ state can be further split into e and f parity components by the spin-rotation and Jahn-Teller interactions. The selection rule ($\Delta J=0,\pm 1$) gives rise to 12 possible branches identified by the branch notation $^{\Delta K}\Delta J_{F'_iF''_j}$ ($i=1,2;j=1,2$).

used to assign J and K values to each of the 18 possible branches of this spin-orbit component. Branch assignments in the $K'=0\leftarrow K''=1$ and $K'=2\leftarrow K''=1$ subbands were facilitated by the unresolved parity doubling in the $K'=0$ and $K'=2$ levels of the $\tilde{A}\,^2E$ state. This proved helpful because, for example, in the $K'=2\leftarrow K''=1$ subband, the position of the $^rR_{12}$ branch can only be predicted from the $^rP_{12}$ or $^rQ_{11}$ branches if the parity doubling is not negligible. However, if the parity splitting is unresolved, then any of the five remaining branches of this subband can be used to predict the location of this branch. The observation of first lines aided in the unambiguous assignment of K' values.[17] For the $\tilde{A}\,^2E_{3/2}$-$\tilde{X}\,^2A_1$ spin-orbit component, identification of the branches proceeded by the same method as for the $\tilde{A}\,^2E_{1/2}$-$\tilde{X}\,^2A_1$ component. In addition, line assignments in this component were aided by the almost negligible parity splitting in the $K'=1$ state. As a result, branches in the $K'=1\leftarrow K''=0$ subband could be related in a similar manner as the $K'=0\leftarrow K''=1$ and $K'=2\leftarrow K''=1$ subbands, in which the parity splitting is unresolved.

A total of 186 lines in 35 of the 36 possible branches from the three ΔK subbands of the two spin-orbit components were identified and assigned for the $\tilde{A}\,^2E$-$\tilde{X}\,^2A_1$ transition of $SrCH_3$. These data can be found in Ref. 32. A portion of the $\tilde{A}\,^2E_{1/2}$-$\tilde{X}\,^2A_1$ spectrum, with line assignments, is shown in Fig. 5. Fifteen of the 18 possible branches in the three ΔK subbands of this spin-orbit component are shown

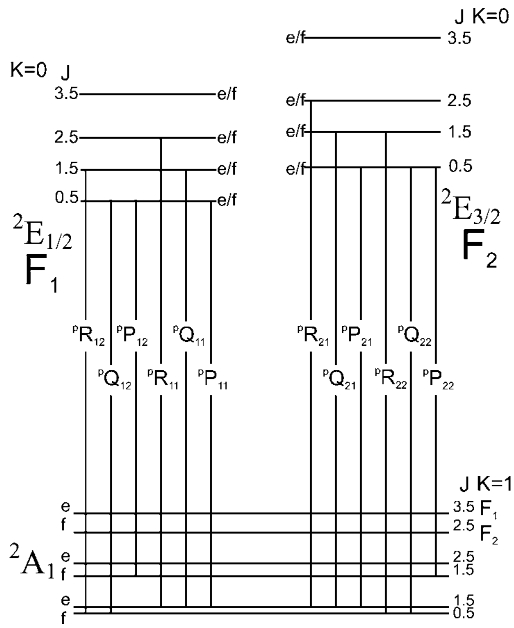

FIG. 3. An energy level diagram showing the allowed transitions of the $K'=0 \leftarrow K''=1$ subband of the $\tilde{A}\,^2E$-$\tilde{X}\,^2A_1$ transition of $SrCH_3$. Each rotational level is labeled by the symmetric top quantum numbers J and K. The $\tilde{X}\,^2A_1$ state is split into two spin states by the spin-rotation interaction, and the $\tilde{A}\,^2E$ state is split into two components $^2E_{1/2}$ (F_1) and $^2E_{3/2}$ (F_2) by spin-orbit coupling. The parity splitting of the $K'=0(K'_R=1)$ levels of the $\tilde{A}\,^2E$ state was found to be negligible. Allowed transitions in this subband are indicated by the branch notation $^{\Delta K}\Delta J_{F'_iF''_j}$ $(i=1,2; j=1,2)$.

here, identified by the branch notation $^{\Delta K}\Delta J_{F'_iF''_j}$ $(i=1,2; j=1,2)$. Transitions arising from the $K'=1 \leftarrow K''=0$ subband are labeled on top in italics, while those from the $K'=0 \leftarrow K''=1$ and $K'=2 \leftarrow K''=1$ subbands are shown below. Each individual rotational line is labeled by its J value. The similar band origin of each of the ΔK subbands causes the spectrum to appear congested.

IV. ANALYSIS

The $\tilde{A}\,^2E$-$\tilde{X}\,^2A_1$ transition data of $SrCH_3$ were modeled using the effective Hamiltonian,[4,5,8,15]

$$\hat{\mathbf{H}}_{\mathrm{Eff}} = \hat{\mathbf{H}}_{\mathrm{Rot}} + \hat{\mathbf{H}}_{\mathrm{CD}} + \hat{\mathbf{H}}_{\mathrm{SR}} + \hat{\mathbf{H}}_{\mathrm{SO}} + \hat{\mathbf{H}}_{\mathrm{Cor}} + \hat{\mathbf{H}}_{\mathrm{JT}}, \tag{1}$$

in which the individual terms describe the rotational motion of the molecule ($\hat{\mathbf{H}}_{\mathrm{Rot}}$), the centrifugal distortion to the rotation ($\hat{\mathbf{H}}_{\mathrm{CD}}$), the spin-rotation interaction ($\hat{\mathbf{H}}_{\mathrm{SR}}$), the spin-orbit coupling ($\hat{\mathbf{H}}_{\mathrm{SO}}$), the Coriolis effect ($\hat{\mathbf{H}}_{\mathrm{Cor}}$), and the Jahn-Teller (**L**-uncoupling) interactions ($\hat{\mathbf{H}}_{\mathrm{JT}}$). The final three terms in Eq. (1) were set to zero to model the $\tilde{X}\,^2A_1$ state, and the entire expression was used to describe the $\tilde{A}\,^2E$ state. This Hamiltonian was incorporated into a least squares fitting program using the matrix elements of Endo *et al.* in a Hund's case (a) basis.[8]

Initially, the optical data were fit using the rotation (A, B), spin-orbit ($a\zeta_e d$, $a_D\zeta_e d$), spin-rotation (ε_{aa}, $\varepsilon_{bc}=(\varepsilon_{bb}+\varepsilon_{cc})/2$, ε_1), Coriolis ($A\zeta_t$), and Jahn-Teller (h_1) terms in the $\tilde{A}\,^2E$ state. The ground state constants were fixed to previously determined values.[24] In this initial fitting, the constants

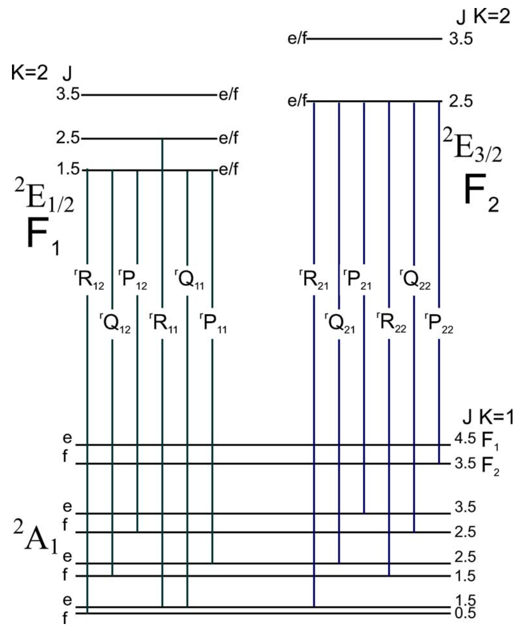

FIG. 4. The allowed transitions of the $K'=2 \leftarrow K''=1$ subband of the $\tilde{A}\,^2E$-$\tilde{X}\,^2A_1$ transition of $SrCH_3$ are shown. Each rotational level is labeled by the symmetric top quantum numbers J and K. The two spin-rotation states of the $\tilde{X}\,^2A_1$ state are labeled as F_1 and F_2, and the two spin-orbit levels of the $\tilde{A}\,^2E$ are identified as $^2E_{1/2}$ (F_1) and $^2E_{3/2}$ (F_2). For the $K'=2$ state, the parity splitting of the rotational levels was not resolved. Transitions are labeled by the branch notation $^{\Delta K}\Delta J_{F'_iF''_j}$ $(i=1,2;\ j=1,2)$.

h_1 and ε_{bc} could not be ascertained reliably from our data set. Interestingly, these parameters were determined in the analysis of the high resolution spectrum of the $\tilde{A}\,^2E$-$\tilde{X}\,^2A_1$ transition of $CaOCH_3$.[18,19] As a result, we performed a fit of the $CaOCH_3$ data using our least squares fitting program and found our program reproduced the previous values. However, when the more extensive $CaOCH_3$ data set was reduced

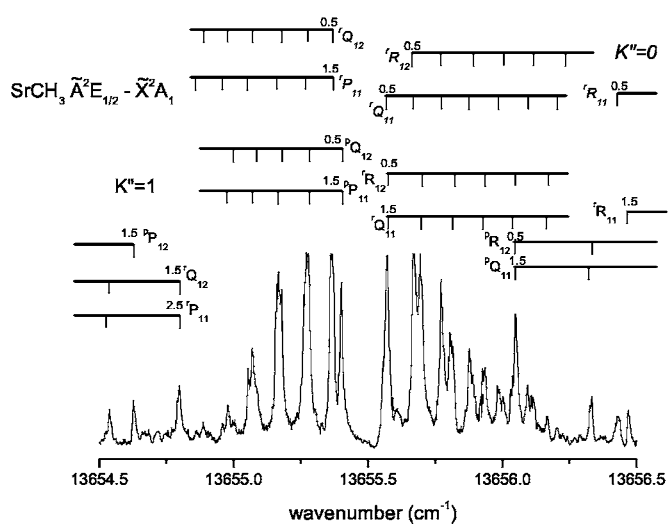

FIG. 5. A portion of the high-resolution spectrum of the $\tilde{A}\,^2E_{1/2}$-$\tilde{X}\,^2A_1$ spin-orbit component of $SrCH_3$ is shown near the origin. Transitions in 15 of the 18 branches assigned to the $K'=0 \leftarrow K''=1$ subband (on top in italics) and the $K'=0 \leftarrow K''=1$ and $K'=2 \leftarrow K''=1$ subbands (on bottom) are present. Individual rotational lines are labeled by their J values in addition to the branch notation $^{\Delta K}\Delta J_{F'_iF''_j}$ $(i=1,2;\ j=1,2)$. The three subbands have similar band origins, which results in a congested spectrum.

TABLE I. Spectroscopic constants (in cm^{-1}) for the $\tilde{A}\,^2E$ and $\tilde{X}\,^2A_1$ states of $SrCH_3$.

Constant[a]	$\tilde{X}\,^2A_1$	$\tilde{A}\,^2E$
T	0.0	13 800.3762(9)
$a\zeta_e d$		279.1651(17)
$a_D\zeta_e d$		−0.0297(15)
$A\zeta_t$		5.248 33(83)
A	5.390[b]	5.334 94(75)
B	0.193 833 336(16)	0.195 068(21)
D_N	$2.148\,93(11)\times10^{-7}$	
D_{NK}	$1.613\,49(51)\times10^{-5}$	
H_{NK}	$2.920(21)\times10^{-10}$	
H_{KN}	$3.18(43)\times10^{-9}$	
ε_{aa}	0.000 883(34)	0.3692(33)
ε_{bc}	0.004 128 52(43)	
ε_1		−0.094 15(12)

[a]Values in parenthesis are 1σ standard deviations, in units of the last significant digits.
[b]Fixed to theoretical value (Ref. 33).

to include only the same J values from the same ΔK subbands observed in our current study of $SrCH_3$, h_1 and ε_{bc} could not be obtained reliably. In order to determine h_1 and ε_{bc} from the $CaOCH_3$ data set, we found that lines with $J' > 9.5$ had to be included in the fit. As a result, h_1 and ε_{bc} were both fixed to zero in subsequent fits of the $\tilde{A}\,^2E$-$\tilde{X}\,^2A_1$ transition data of $SrCH_3$. In addition, because of the low J values ($J' \leq 8.5$) observed in our spectra, the centrifugal distortion terms (D_N, D_{NK}, and D_K) in the $\tilde{A}\,^2E$ state were also fixed to zero. All 186 assigned rotational lines from the three ΔK subbands of the $\tilde{A}\,^2E$-$\tilde{X}\,^2A_1$ transition and the 137 pure rotational lines of the $\tilde{X}\,^2A_1$ state[31] were included in the final fit, in which all of the ground state constants, except A, were allowed to vary. The A rotational constant in the ground state was fixed to the theoretical value,[33] because no previous experimental value was available and no transitions, where $\Delta K_R \neq 0$, were observed in this work. The two data sets were weighted according to their experimental uncertainties: 0.005 cm^{-1} for the optical data and 60 kHz for the pure rotational data. The spectroscopic constants for the $\tilde{A}\,^2E$ and $\tilde{X}\,^2A_1$ states derived from this final fit are listed in Table I.

V. DISCUSSION

The energy separation of the two spin-orbit components of the $\tilde{A}\,^2E$ state is given by the constant $a\zeta_e d$. Within this parameter, a describes the magnitude of the spin-orbit coupling, ζ_e is the projection of the electronic angular momentum $\mathbf{L}$ onto the symmetry axis, and d is the Jahn-Teller quenching parameter ($1>|d|>0$). The magnitude of these terms can be estimated by comparing $a\zeta_e d$ with the spin-orbit constant A of other linear strontium containing molecules such as SrOH (A=263.5878 cm^{-1}) (Ref. 34) and SrCCH (A=272.1886 cm^{-1}) (Ref. 29) in their $\tilde{A}\,^2\Pi$ states. These values of A are quite similar to $a\zeta_e d$ (279.1651 cm^{-1}) in the $\tilde{A}\,^2E$ state of $SrCH_3$. Therefore, we can conclude that the quantity $\zeta_e d$ must be close to 1. As mentioned before, for a ^2E state derived predominantly from a p orbital, such as the case for the $\tilde{A}\,^2E$ state of $SrCH_3$ ($5p$), ζ_e is expected to be close to 1. In this scenario, d must also be approximately 1, which indicates that the Jahn-Teller distortion is small in the lowest vibrational level of the $\tilde{A}\,^2E$ state. If the Jahn-Teller interaction is neglected and hence d=1, then a value of ζ_e can be estimated using the following equation:[15]

$$\zeta_t = \zeta_e d + \frac{1-d}{2}\zeta_2, \tag{2}$$

in which ζ_t is the projection of the vibronic angular momentum onto the symmetry axis, and ζ_2 is the vibrational Coriolis coupling coefficient for the Jahn-Teller active degenerate vibrational mode. From this equation, if d=1, then ζ_t must equal to ζ_e. Using the values of A (rotational constant) and $A\zeta_t$ for the ground vibrational level of the $\tilde{A}\,^2E$ state found in Table I, ζ_t is calculated to be 0.9838. The value of ζ_e (0.9838) for the $\tilde{A}\,^2E$ state is in very good agreement with the expected value of 1. Finally, assuming d=1 and using ζ_e=0.9838 and $a\zeta_e d$=279.1651 cm^{-1}, the magnitude of the spin-orbit coupling constant in the $\tilde{A}\,^2E$ state is estimated to be a=283.772 cm^{-1}.

The spin rotation parameter ε_{aa} for the $\tilde{A}\,^2E$ state of $SrCH_3$ can be estimated by considering the second order contribution to this parameter arising from spin-orbit coupling. For molecules containing heavy atoms, the first order contribution to the spin-rotation parameter is typically much smaller than the second order portion and may be neglected.[12] The second order spin-orbit contribution to ε_{aa} is composed of two factors; electronic ($\varepsilon_{aa}^{(2e)}$) and vibrational ($\varepsilon_{aa}^{(2v)}$).[12,35] The vibrational term is dominated by the Jahn-Teller interaction, which was previously shown to be small in the $\tilde{A}\,^2E$ state of $SrCH_3$, and will be ignored. The electronic contribution can be approximated using second order perturbation theory and has the following form for a nonlinear molecule,[36]

$$\varepsilon_{aa}^{(2)} = -\sum_{\alpha\neq\alpha'} \frac{4\langle\alpha|aL_z|\alpha'\rangle\langle\alpha'|AL_z|\alpha\rangle}{E_\alpha - E_{\alpha'}}, \tag{3}$$

where α' is the electronic state of interest, α are other perturbing electronic states, and E is the state energy. Equation (3) can be simplified by assuming that the $\tilde{A}\,^2E$ state interacts with a single dominant perturbing state of the correct symmetry, thereby removing the sum over α (unique perturber approximation). For $SrCH_3$, the closest possible perturbing state is the $\tilde{E}\,^2E$ state (the $\tilde{C}\,^2E$ state arises from metal $d\delta$ orbitals, corresponding to a $^2\Delta$ state in the linear limit and cannot connect to the $\tilde{A}\,^2E$ state). If we approximate $\langle\tilde{A}^2E|L_z|\tilde{E}\,^2E\rangle$ as $\zeta_e d$ then the expression for $\varepsilon_{aa}^{(2)}$ is reduced to

$$\varepsilon_{aa}^{(2)} = -\frac{4\langle \tilde{A}\,{}^2E|aL_z|\tilde{E}\,{}^2E\rangle\langle \tilde{A}\,{}^2E|AL_z|\tilde{E}\,{}^2E\rangle}{E_{\tilde{A}\,{}^2E} - E_{\tilde{E}\,{}^2E}} = -\frac{4a\zeta_e dA\zeta_e d}{E_{\tilde{A}\,{}^2E} - E_{\tilde{E}\,{}^2E}} = -\frac{4a\zeta_e dA\zeta_t}{E_{\tilde{A}\,{}^2E} - E_{\tilde{E}\,{}^2E}}. \quad (4)$$

Unfortunately, the energy separation between the $\tilde{A}\,{}^2E$ and $\tilde{E}\,{}^2E$ states in $SrCH_3$ is not known. For $CaCH_3$, Ortiz[37] has calculated the energy of the $\tilde{E}\,{}^2E$ state resulting in a $\tilde{A}\,{}^2E$-$\tilde{E}\,{}^2E$ splitting of $\sim$13 930 cm^{-1}. Using this energy separation as an estimate for $SrCH_3$ and the values of $a\zeta_e d$ (279.1651 cm^{-1}) and $A\zeta_t$ (5.248 33 cm^{-1}), $\varepsilon_{aa}^{(2)}$ is calculated to be 0.4207 cm^{-1}. This value is in very reasonable agreement with the experimentally determined constant (0.3692 cm^{-1}), considering the assumptions made in deriving Eq. (4) and estimating the $\tilde{A}\,{}^2E$-$\tilde{E}\,{}^2E$ energy splitting from $CaCH_3$.

The higher-order spin-rotation parameter ε_1 can also be calculated by considering second order contributions arising from spin-orbit coupling. Using the pure precession relationship and the unique perturber approximation the following expression for ε_1 has been derived[5,16]

$$\varepsilon_1 = \frac{aB\ell(\ell+1)}{E_{\tilde{A}\,{}^2E} - E_{\tilde{B}\,{}^2A_1}}, \quad (5)$$

where ℓ is the atomic orbital angular momentum. Using the values a=283.772 cm^{-1}, B=0.195 068 cm^{-1}, $E(\tilde{A}\,{}^2E)$ =13 800.3762 cm^{-1}, and $E(\tilde{B}{}^2A_1)$=14 787.581 34 cm^{-1} (Ref. 24), and assuming that the $\tilde{A}\,{}^2E$ state arises solely from a p atomic orbital (ℓ=1), ε_1 is estimated to be −0.1121 cm^{-1}. This value has the same sign but is approximately 20% larger than the experimentally determined parameter (−0.094 15 cm^{-1}). Aside from the assumptions made in the derivation of this expression, this difference may indicate that the $\tilde{A}\,{}^2E$ state is not composed entirely of p orbital character; d orbitals may be mixing in.

It has also been shown that ε_1 is analogous to the Λ-doubling constant p in $^2\Pi$ states. The two parameters are related by the expression $\varepsilon_1 = p/2$.[5] If we compare $2\varepsilon_1$= −0.1883 cm^{-1} in the $\tilde{A}\,{}^2E$ state of $SrCH_3$, with the p values in the $\tilde{A}\,{}^2\Pi$ state of other linear strontium containing molecules such as SrOH (−0.143 289 cm^{-1}) (Ref. 34) and SrCCH (−0.1101 cm^{-1}) (Ref. 29), we find that they are quite similar. This is not unexpected as the electronic structure of these molecules is mostly derived from the Sr^+ ion and is not expected to change dramatically with different ligands.

From the rotational constants shown in Table I, the structure of $SrCH_3$ in the $\tilde{A}\,{}^2E$ state can be estimated. Because no isotopologue data exist for the $\tilde{A}\,{}^2E$ state, the C–H bond length was held fixed to the ground state theoretical value.[33] This assumption is reasonable, because the C–H bond length should exhibit the smallest change upon electronic excitation.[18] In addition, the A rotational constant in the ground state was fixed to the theoretical value;[33] therefore, the A value determined in the $\tilde{A}\,{}^2E$ state is a measure of the change in A from the ground state. In order to ensure that differences in the rotational constants between the ground and excited electronic states are due only to changes in geometry, second order spin-orbit contributions must be considered. For the $\tilde{A}\,{}^2E$ state of $CaCH_3$ the second order contributions were found to comprise only $\sim$0.35% of the value of the A rotational constant.[17] A similar calculation for the $\tilde{A}\,{}^2E$ state of $SrCH_3$ shows that the second order contributions to the rotational parameters, A and B, are less then 0.25% of the total value and may be safely ignored. The estimated structural parameters of the $\tilde{X}\,{}^2A_1$ and $\tilde{A}\,{}^2E$ states of $SrCH_3$ are shown in Table II along with those of the $\tilde{B}\,{}^2A_1$ state for comparison. The Sr–C bond length was found to decrease slightly ($\sim$0.006 Å) upon promotion of the unpaired electron from the $\tilde{X}\,{}^2A_1$ state to the $\tilde{A}\,{}^2E$ state. A decrease in the metal-ligand bond length between the $\tilde{A}\,{}^2\Pi$ and $\tilde{X}{}^2\Sigma^+$ states has also been observed in other strontium polyatomic molecules such as SrOH ($\sim$0.02 Å) (Ref. 34) and SrCCH ($\sim$0.03 Å) (Ref. 29). This bond length shortening has been attributed to the slight polarization of the unpaired electron away from the ligand in the $p\pi$ orbital ($\tilde{A}\,{}^2E$ state) as compared to the $s\sigma$ orbital ($\tilde{X}\,{}^2A_1$ state). As a result, the electrostatic interaction between the strontium cation and anionic ligand increases and the metal-ligand bond length shortens. In addition, the polarization of the unpaired electron away from the ligand allows more room for the CH_3 umbrella to open. In Table II, the H–C–H bond angle is found to increase by $\sim$0.8° between the $\tilde{X}\,{}^2A_1$ and $\tilde{A}\,{}^2E$ states of $SrCH_3$. This behavior is similar to the $\sim$0.9° increase observed in the $\tilde{A}\,{}^2E$ state of $CaCH_3$ as compared to the ground state.[17] In $SrCH_3$ (as in $CaCH_3$) these structural differences are very small, and the metal-ligand bond length change is less than observed for the corresponding transitions in SrOH and SrCCH.

TABLE II. Structural parameters for $SrCH_3$.

State	Parameter	$SrCH_3$[a]
$\tilde{X}\,{}^2A_1$	$r_{M\text{–}C}$ (Å)	2.487
	$r_{C\text{–}H}$ (Å)[b]	1.104
	$\theta_{H\text{–}C\text{–}H}$ (°)	105.8
$\tilde{A}\,{}^2E$	$r_{M\text{–}C}$ (Å)	2.481
	$r_{C\text{–}H}$ (Å)[b]	1.104
	$\theta_{H\text{–}C\text{–}H}$ (°)	106.6
$\tilde{B}\,{}^2A_1$	$r_{M\text{–}C}$ (Å)	2.492
	$r_{C\text{–}H}$ (Å)[b]	1.104
	$\theta_{H\text{–}C\text{–}H}$ (°)	107.0

[a]Value of A in ground state fixed to theoretical value (Ref. 33).
[b]Fixed to theoretical value (Ref. 33).

VI. CONCLUSION

A high-resolution spectrum of the $\tilde{A}\,{}^2E$-$\tilde{X}\,{}^2A_1$ electronic transition of $SrCH_3$ has been recorded using laser excitation spectroscopy. Rotational and fine structure parameters for the $\tilde{A}\,{}^2E$ state were determined in a rotational analysis of the data. The Jahn-Teller effect was found to be small in the lowest vibrational level of the $\tilde{A}\,^2E$ state. Estimates of the spin-rotation parameters from pure precession expressions are in good agreement with the experimentally determined values and indicate that the $\tilde{A}\,^2E$ state is not entirely composed of p character. From the rotational constants, the structure of $SrCH_3$ in the $\tilde{A}\,^2E$ state has been estimated. The metal-ligand bond length was found to decrease slightly in the $\tilde{A}\,^2E$ state from the $\tilde{X}\,^2A_1$ state, similar to, but less than, other strontium containing radicals.

ACKNOWLEDGMENTS

Financial support for this work was provided by the Natural Sciences and Engineering Research Council (NSERC) of Canada. In addition, the authors would like to thank Dr. C. Linton and Dr. P. Crozet for giving us a copy of their symmetric top fitting program, which allowed us to compare and confirm the results from our fitting program.

[1] P. F. Bernath, *Advances in Photochemistry* (Wiley, New York, 1997), Vol. 23, p. 1.
[2] A. M. Ellis, Int. Rev. Phys. Chem. **20**, 551 (2001).
[3] H. A. Jahn and E. Teller, Proc. R. Soc. London, Ser. A **161**, 220 (1937).
[4] J. M. Brown, Mol. Phys. **20**, 817 (1971).
[5] J. T. Hougen, J. Mol. Spectrosc. **81**, 73 (1980).
[6] J. K. G. Watson, J. Mol. Spectrosc. **103**, 125 (1984).
[7] G. W. King and C. H. Warren, J. Mol. Spectrosc. **32**, 138 (1969).
[8] Y. Endo, S. Saito, and E. Hirota, J. Chem. Phys. **81**, 122 (1984).
[9] T. Momose, Y. Endo, E. Hirota, and T. Shida, J. Chem. Phys. **88**, 5338 (1988).
[10] S. C. Foster, P. Misra, T.-Y. D. Lin, C. P. Damo, C. C. Carter, and T. A. Miller, J. Phys. Chem. **92**, 5914 (1988).
[11] X. Liu, C. P. Damo, T.-Y. D. Lin, S. C. Foster, P. Misra, L. Yu, and T. A. Miller, J. Phys. Chem. **93**, 2266 (1989).
[12] X. Liu, S. C. Foster, J. M. Williamson, L. Yu, and T. A. Miller, Mol. Phys. **69**, 357 (1990).
[13] Y.-C. Hsu, X. Liu, and T. A. Miller, J. Chem. Phys. **90**, 6852 (1989).
[14] L. Yu, S. C. Foster, J. M. Williamson, M. C. Heaven, and T. A. Miller, J. Phys. Chem. **92**, 4263 (1988).
[15] R. Rubino, J. M. Williamson, and T. A. Miller, J. Chem. Phys. **103**, 5964 (1995).
[16] C. R. Brazier and P. F. Bernath, J. Chem. Phys. **91**, 4548 (1989).
[17] A. J. Marr, F. Grieman, and T. C. Steimle, J. Chem. Phys. **105**, 3930 (1996).
[18] P. Crozet, F. Martin, A. J. Ross, C. Linton, M. J. Dick, and A. G. Adam, J. Mol. Spectrosc. **213**, 28 (2002).
[19] P. Crozet, A. J. Ross, C. Linton, A. G. Adam, W. S. Hopkins, and R. J. LeRoy, J. Mol. Spectrosc. **229**, 224 (2005).
[20] L. C. O'Brien, C. R. Brazier, and P. F. Bernath, J. Mol. Spectrosc. **130**, 33 (1988).
[21] T. M. Cerny, X. Q. Tan, J. M. Williamson, E. S. J. Robles, A. M. Ellis, and T. A. Miller, J. Chem. Phys. **99**, 9376 (1993).
[22] M. B. Pushkarsky, T. A. Barckholtz, and T. A. Miller, J. Chem. Phys. **110**, 2016 (1999).
[23] T. A. Barckholtz and T. A. Miller, Int. Rev. Phys. Chem. **17**, 435 (1998).
[24] P. M. Sheridan, M. J. Dick, J.-G. Wang, and P. F. Bernath, J. Phys. Chem. A **109**, 10547 (2005).
[25] C. Zhao, P. G. Hajigeorgiou, P. F. Bernath, and J. W. Hepburn, J. Mol. Spectrosc. **176**, 268 (1996).
[26] C. R. Brazier and P. F. Bernath, J. Chem. Phys. **86**, 5918 (1987).
[27] S. Gerstenkorn, J. Verges, and J. Chevillard, *Atlas du Spectre d'Absorption de la Molécule d'Iode* (Laboratoire Aimé-Cotton, CNRS 91405, Orsay, France, 1982).
[28] S. Gerstenkorn and P. Luc, *Atlas du Spectre d'Absorption de la Molécule d'Iode* (Laboratoire Aimé-Cotton, CNRS 91405, Orsay, France, 1978).
[29] M. J. Dick, P. M. Sheridan, J.-G. Wang, and P. F. Bernath, J. Mol. Spectrosc. **233**, 197 (2005).
[30] C. H. Townes and A. L. Schawlow, *Microwave Spectroscopy* (Dover, New York, 1975).
[31] M. A. Anderson, J. S. Robinson, and L. M. Ziurys, Chem. Phys. Lett. **257**, 471 (1996).
[32] See EPAPS Document No. E-JCPSA6-124-010614 for a complete list of the measured transition frequencies of the $\tilde{A}\,^2E$-$\tilde{X}\,^2A_1$ electronic transition of $SrCH_3$. This document can be reached via a direct link in the online article's HTML reference section or via the EPAPS homepage (http://www.aip.org/pubservs/epaps.html).
[33] W.-T. Chan and I. P. Hamilton, Chem. Phys. Lett. **297**, 217 (1998).
[34] J.-G. Wang, P. M. Sheridan, M. J. Dick, and P. F. Bernath, J. Mol. Spectrosc. **236**, 21 (2006).
[35] X. Liu, L. Yu, and T. A. Miller, J. Mol. Spectrosc. **140**, 112 (1990).
[36] R. N. Dixon, Mol. Phys. **10**, 1 (1965).
[37] J. V. Ortiz, J. Chem. Phys. **92**, 6728 (1990).